

Detection of Earth-mass and Super-Earth Trojan Planets Using Transit Timing Variation Method

Nader Haghighipour
Stephanie Capen
Tobias C. Hinse

the date of receipt and acceptance should be inserted later

Abstract We have carried out an extensive study of the possibility of the detection of Earth-mass and super-Earth Trojan planets using transit timing variation method with the *Kepler* space telescope. We have considered a system consisting of a transiting Jovian-type planet in a short period orbit, and determined the induced variations in its transit timing due to an Earth-mass/super-Earth Trojan planet. We mapped a large section of the phase space around the 1:1 mean-motion resonance and identified regions corresponding to several other mean-motion resonances where the orbit of the planet would be stable. We calculated TTVs for different values of the mass and orbital elements of the transiting and perturbing bodies as well as the mass of central star, and identified orbital configurations of these objects (ranges of their orbital elements and masses) for which the resulted TTVs would be within the range of the variations of the transit timing of *Kepler*'s planetary candidates. Results of our study indicate that in general, the amplitudes of the TTVs fall within the detectable range of timing precision obtained from the *Kepler*'s long-cadence data, and depending on the parameters of the system, their magnitudes may become as large as a few hours. The probability of detection is higher for super-Earth Trojans with slightly eccentric orbits around short-period Jovian-type planets with masses slightly smaller than Jupiter. We present the details of our study and discuss the implications of its results.

Keywords Planetary Systems · Stability · Phase Space Structure · Resonance · Periodic Orbits · Numerical Method

N. Haghighipour
Institute for Astronomy and NASA Astrobiology Institute, University of Hawai'i-Manoa, 2680 Woodlawn Drive, Honolulu, HI 96822, USA, Tel.: +1-808-956-6098, Fax: +1-808-956-4351, E-mail: nader@ifa.hawaii.edu
S. Capen
Department of Education, University of Hawai'i-Manoa, Honolulu, HI 96822, USA, E-mail: stephaniecapen@gmail.com.
T. C. Hinse
Korea Astronomy and Space Science Institute, 304-358 Daejeon, Republic of Korea, and Armagh Observatory, College Hill, BT61 9DG, Armagh, UK E-mail: tchinse@gmail.com

1 Introduction

It is generally accepted that similar to the giant planets of our solar system, Jovian-type exoplanets can host satellites and may have co-orbital and/or Trojan bodies. During the past decade, these considerations have led to initiatives on both modeling the formation of these objects (especially in system with close-in giant planets) and assessing their detectability in particular using ground-based observational facilities. The success of the *Kepler* space telescope in detecting several planets using transit timing variation (TTV) method, combined with the unprecedented photometric sensitivity of this telescope and its high observing cadence has raised the question that whether Trojan planets and satellites of giant exoplanets can also be detected by the *Kepler*. In this paper, we address this question and study the prospects of the detection of these objects by comparing their induced transit timing variations with the transit timing precision of planetary candidates that have been identified by the *Kepler* space telescope.

Since the discovery of the first extrasolar planet, many efforts have been made to develop models for the detection of the satellites of these objects. Sartoretti and Schneider (1999) were the first to study the possibility of the detection of exomoons using transit photometry. Deeg (2002) extended this analysis to smaller objects and examined the photometric detectability of terrestrial-size satellites. Subsequently, Simon et al (2007) studied the transit timing variations induced by exo-satellites as a mechanism for the indirect detection of these bodies. More recently, in a series of articles, Kipping has shown that the measurements of the variations in the time as well as the duration of the transit will allow for the detection and determining the mass of the exomoon of a transiting giant planet (Kipping 2009a&b, 2011).

Efforts have also been made to determine the possibility of the detection of co-orbital and Trojan planets. It has been shown by Laughlin and Chambers (2002) that a pair of Jupiter-like planets in a 1:1 mean-motion resonance (MMR) in a system similar to that of GJ 876 can generate stellar radial velocities with amplitudes ranging from 50 m/s to over 100 m/s. These results agree with the more recent findings of Giuppone et al (2012) who studied the origin and RV-detectability of co-orbital planets. Laughlin and Chambers (2002) showed that as this range of radial velocity falls within the sensitivity of ground-based telescopes, 1:1 resonant planets can be detected using the Doppler Velocimetry technique when the fitting routine takes into account the mutual interactions of these objects.

The detectability of Trojan planets have also been studied by Ford and Gaudi (2006). These authors showed that the perturbation of a planet in the L_4 or L_5 Lagrangian points of a transiting Jovian-type body can cause the time when the stellar RV coincides with the RV of the barycenter of the star-transiting planet system to differ from the time of the planet's mid-transit. As a result, a Trojan planet can create a time offset between the ephemerides obtained from RV and transit photometry. As shown by these authors, these variations present a potential pathway for detecting terrestrial-mass Trojans using ground-based telescopes. In a subsequent article, Ford and Holman (2007) examined the sensitivity of transit timing observations as a mechanism for detecting Trojan planets, and showed that the transit timing variations induced by a terrestrial-class Trojan may fall within the range of the photometric sensitivity of ground-based observational facilities.

The above-mentioned vast interest in the discovery of Trojan planets has roots in the fact that while the theories of planetary dynamics support the existence of

these objects, no Trojan planet exists in our solar system. As such, the detection of these bodies will be a novelty that will have profound effects on the models of planet formation and dynamics. Also, given that many giant planets reside in the habitable zones of their host stars, the Trojans (and satellites) of these objects, if existed and of terrestrial-size, could be potentially habitable. While these characteristics of Trojan planets make them interesting subjects for observational surveys, and although previous studies suggest that these objects are detectable using the current ground-based observing facilities, no Trojan planet has yet been found. The latter may be the indication of the inefficiency of ground-based surveys in searching for this type of planets. The space-based telescopes, especially *Kepler*, on the other hand, have been able to detect many planetary bodies of different sizes using transit photometry and transit timing variation method (Holman et al 2010; Nesvorný et al 2012). From these two techniques, TTV is particularly efficient in detecting Earth-mass and super-Earth planets, especially when these objects are in mean-motion resonance with their corresponding transiting bodies (Agol et al 2005, 2007; Holman and Murray 2005; Steffen and Agol 2005; Heyl and Gladman 2007; Haghighipour and Kirste 2011; Veras et al 2011). The latter makes the foundation of our study. We consider systems with transiting giant planets in short-period orbits, and study the prospects of the detection of putative Earth-mass and super-Earth Trojans using transit timing variations method with the *Kepler* space telescope.

Our approach is numerical and based on calculating TTVs and comparing their amplitudes with the amplitudes of the variations in the transit timing of the *Kepler*'s planetary candidates as reported by Ford et al (2011). We begin by studying the stability of our Trojan planets and identifying the regions of the phase space, in particular resonances around 1:1 MMR, where the orbit of the planet is stable. We then calculate TTVs for the 1:1 MMR configurations, assuming that an Earth-mass or super-Earth Trojan exists in those stable regions. In this paper, we will not be concerned with the formation of Trojans and how our Trojan planets acquired their orbits. Instead, we will focus our study on merely identifying regions of the parameter space for which the amplitudes of TTVs fall within the range of the TTVs of the planetary candidates detected by the *Kepler*. We will also not intend to break the inherent degeneracy associated with the TTV method. Whether an actually observed TTVs is due to a Trojan or a non-Trojan planet is a topic that may require employing other observational techniques, and is outside the scope of this paper.

The rest of this paper is outlined as follows. In section 2, we present the results of our stability analysis and the mapping of the phase space. Section 3 has to do with the calculations of TTVs for different values of the mass and orbital elements of the transiting and Trojan planets. Section 4 concludes this study by reviewing the results and discussing their implications.

2 Numerical Set Up and Stability Analysis

We consider a co-planar system consisting of a star, a transiting planet, and a perturbing body. The mass of the central star is chosen to be between 0.1 and 1 solar-masses (M_{\odot}). The transiting planet is considered to be in a circular orbit with a mass ranging from 0.1 to 1 Jupiter-mass (M_J). The orbital period of this object is taken to be between 3 and 10 days. The perturbing body is a super-Earth ($1M_{\oplus} \leq m_p \leq 10M_{\oplus}$) and its initial orbital eccentricity is chosen from the range of 0 to 0.8 in steps of 0.05.

For the sake of completeness, we start by studying the stability of the two planets in a 1:1 MMR. We used the chaos indicator MEGNO (Mean Exponential Growth factor of Nearby Orbits, Cincotta and Simó 2000, Goździewski 2001) and integrated the three-body system of the star and the transiting and perturbing planets for different combinations of the mass and mean-anomaly of the two planets. Integrations were carried out for more than 100,000 orbits of the transiting body and were terminated when MEGNO reached a value of 10 or larger. For quasi-periodic orbits, MEGNO will asymptotically approach the value of 2.0 and it diverges away from 2.0 exponentially in the case of chaotic orbits. More details on MEGNO and its application to orbital stability of our systems can be found in the appendix.

Figures 1 and 2 show samples of the results for different initial configurations of the two planets. The central stars in these figures are $1 M_{\odot}$ and $0.3 M_{\odot}$, respectively. The transiting planet in each system is Jupiter-mass and in a 4-day orbit in figure 1 and 7.5-day orbit in figure 2. The perturbing body has a mass of $1 M_{\oplus}$. Both three-body systems were considered to be co-planar and the initial values of the longitudes of ascending nodes and arguments of pericenters of the transiting and perturbing planets were set to zero. For more studies on the stability of co-orbital planets and their configurations and orbital elements, we refer the reader to Hadjidemetriou et al (2009, 2011) and Giuppone et al (2010).

Integrations were carried out for different values of the semimajor axis and eccentricity of the perturbing Earth-mass planet. The black curves in each figure show the loci of points for which the orbital perihelion and aphelion distances are at 0.05 AU from the central star. As shown in these figures, in general, the orbit of the perturbing planet is stable when it is entirely outside the influence zone of the transiting body. As expected, however, within the unstable regions, islands of stability appear where the perturbing and transiting planets are in mean-motion resonances. A few of these resonances are shown in figures 1 and 2. We refer the reader to Haghighipour and Kirste (2011) for a detailed analysis of the detectability of an Earth-mass planet with the TTV method in these resonances.

We also carried out similar integrations considering the initial argument of the periastron of the Earth-mass planet to be 60° . A sample of the results, as shown in figure 3, once again indicate that the orbit of the Earth-mass perturber will be stable in close distances to the central star. Islands of stability also appear in this case, in particular for the 1:1 MMR, which shows the Earth-mass planet will be stable for its value of orbital eccentricity up to ~ 0.4 .

An interesting result shown in figures 1 and 2 is the island of stability at the 1:1 MMR. As shown here, the orbit of the Earth-mass perturber may be stable for different values of its eccentricity. We carried out more detailed analysis of the long-term stability of this object and integrated our system using the Bulirsch-Stoer integrator of the N-body integration package MERCURY (Chambers 1999). Figure 4 shows the results for two sample cases where the eccentricity of the perturbing Earth-mass planet is 0.4 and 0.8 (the white crosses in the 1:1 stable region of the top-left panel of figure 1), respectively. Note that the angular orbital elements of these objects are similar to those of the systems in figures 1 and 2. As shown in the top panels of this figure, the Earth-mass planet maintained its orbit for at least one million years suggesting that the quasi-periodic regions in the locations of 1:1 MMRs in figures 1 and 2 are true representation of stable planetary orbits. The bottom panels of this figure show the astrometric orbits of the two planets for one orbit.

We also explored the effect of the orbital eccentricity of the transiting planet on the stability of the Earth-mass object. For these calculations we considered two cases; the real system of M star KOI-254 where a $0.505 M_J$ planet transits a 0.59 solar-mass star in a 2.45-day orbit with an eccentricity of 0.1 (Johnson et al 2011), and a system consisting of a solar-mass star with a transiting Jupiter-mass planet in a 3-day circular orbit. Figures 5 and 6 show the MEGNO maps of an Earth-mass planets in these systems. As seen from figure 5, the slight eccentricity of the transiting planet KOI-254 b has caused almost the entire region of its associated 1:1 MMR to become unstable. However, figure 6 shows that in the system of this figure, an Earth-mass planet can have stable orbits in both L_4 and L_5 Lagrangian points when the eccentricities of both planets are 0.1.

3 Calculation of TTV

To calculate the variations in the transit timing of the giant planet, we first performed similar N-body integrations as those explained above, once with and once without the perturbing Earth-mass body. Integrations were carried out for a time span of 30 years to show both the short-term and long-term effects (we note that for the purpose of detecting TTVs with the *Kepler*, a time span of 3 years will suffice). For each set of simulations, the transit timing variations were calculated by obtaining the difference between the time of mid-transit in the systems with and without the perturbing body. We assumed that at $t = 0$, the centers of the star and the transiting planet were on the x -axis, and calculated the time of transit by interpolating between the times before and after the center of transiting planet crossed the center of the star.

Figure 7 shows a sample of the results. The system in this figure consists of a solar-mass star, a Jupiter-mass transiting planet in a 3-day orbit, and an Earth-mass perturber in the L_4 Lagrangian point. The four panels correspond to the initial orbital eccentricity of the Trojan planet from 0 to 0.15. The initial orbital eccentricity of the transiting planet was set to zero. As shown here, the maximum values of TTV vary from ~ 16 s to ~ 72 s by increasing the eccentricity of the Earth-mass planet. A comparison between the amplitudes of TTVs in figure 7 and the transit timing variations of the planetary candidates identified by the *Kepler* space telescope in Q0-2 indicates that these TTVs fall in the lowest range of the detected transit timings [See figure 1 of Ford et al. (2011); The smallest detected TTV in this figure is slightly larger than 12 seconds].

Figure 7 also shows that as expected, an increase in the orbital eccentricity of the Trojan planet results in an increase in the amplitude of TTVs. This motivated us to examine the change in the magnitude of TTVs for different values of the initial orbital eccentricity of the perturbing planet. As shown in figure 3, the orbit of the Trojan planet becomes unstable for large values of its eccentricity. We, therefore, chose a system similar to that of the top-left panel of figure 1, and calculated TTVs for different values of the orbital eccentricity of the Trojan perturber. Figure 8 shows the results for a time span close to 30 years. As shown here, the amplitudes of TTVs are now within the range of approximately 160 s to 360 s. This range is within the lower limit of the TTVs of the *Kepler's* multiple planet candidates (~ 2 minutes, see figure 1 of Ford et al. 2011) pointing to the large prospect for the detection of these objects within the extended lifetime of the *Kepler*.

We performed similar calculations for different values of the mass of the perturbing body (1–10 Earth-masses), its orbital eccentricity (0–0.15), and the mass and orbital period of the transiting planet. Figure 9 shows the maximum values of the TTVs of a Jupiter-mass planet in a 3-day orbit for four different values of the mass of the Trojan perturber. The central star is solar-mass and the transiting planet was initially in a circular orbit. As expected, the magnitude of TTVs increase, reaching to several minutes, by increasing the mass and eccentricity of the Trojan body. These values are well within the range of the *Kepler's* detected TTVs (~ 8 minutes, Ford et al. 2011) implying reasonable probability of detection for super-Earth Trojans with slight orbital eccentricities. Figure 10 shows similar calculations when the mass of the transiting planet is $0.1 M_J$ and $0.5 M_J$. In these systems, even circular super-Earths induce TTVs that are comparable with the TTVs of some of the *Kepler's* planets such as Kepler-9 b&c (~ 25 minutes to a slightly more than an hours, Holman et al 2010).

The amplitudes of TTVs are significantly increased when the transiting planet is at larger orbits. As shown in figure 11, the maximum values of TTVs vary between approximately 0.6 and 2.3 hours when a $0.1 M_J$ transiting planet in orbits with periods between 3 and 10 days is perturbed by a 6 Earth-mass super-Earth Trojan. Such large TTVs are entirely within the bulk of the TTVs of the *Kepler's* planetary candidates (10–40 minutes, Ford et al. 2011). Figure 12 shows this trend in terms of the mass of the Trojan planet and for different values of the orbital period of the transiting body where the amplitude of TTVs raise up to over 4 hours. Results indicate that in general, super-Earth Trojans with small orbital eccentricities have a reasonably high probability of detection in systems where the transiting planets are slightly smaller than Jupiter and in moderately short-period orbits.

4 Concluding Remarks

We have studied the detectability of Earth-mass Trojans by comparing the variations they induce in the transit timing of their Jovian-type host planets with the detected transit timing variations of *Kepler's* planetary candidates. We analyzed the stability of these systems for different values of the mass and orbital elements of the transiting and perturbing bodies, and calculated their associated TTVs for the ranges of their orbital elements that correspond to their long-term stability. Results indicated that while in general, the amplitude of TTVs fall within the detectable range of timing precision obtained from the *Kepler's* long-cadence data, the prospects of the detection of Trojan planets are higher for super-Earth Trojans in slightly eccentric orbits around transiting Jovian planets with masses smaller than Jupiter. Our study also present a pathway to break the strong degeneracy associated with the RV-detection of Trojan planets around L_4 and L_5 (Giuppone et al 2012) by combining the information obtained from the study of the transits of their systems and their TTVs.

The purpose of our study was to identify regions of the parameter space for which the amplitude of the TTVs of a transiting planet due to the perturbation of its Trojan body would fall within the range of the photometric sensitivity of the *Kepler*. However, whether a detected TTV is actually due to a Trojan planet cannot be deduced from our results. While as shown by Nesvorný and Morbidelli (2008), Nesvorný (2009), Nesvorný and Beauge (2010), and Nesvorný et al (2012), it would be possible in non-resonant systems to determine the mass and orbital elements of the perturbing body by analyzing TTVs alone, to extract the nature of a perturbing Trojan planet from

detected TTVs, one has to either compare the detected TTVs with those in large TTV catalogs (e.g., Haghighipour and Kirste 2011) or complement the detection by using other planet-detection techniques, in particular the radial velocity method (Laughlin and Chambers 2002, Giuppone et al 2012).

We based our study on the assumption that similar to the giant planets of our solar system, extrasolar giant planets may also have Trojans objects and satellites. These objects may be as large as terrestrial planets, in which case their perturbations on the orbital motion of their host planet may become detectable. How such Trojan planets form is a matter of on-going research. In general, one can think of three scenarios; in-situ formation around L_4 and L_5 Lagrangian points of a short-period giant planet, in-situ formation around the host giant planet followed by the inward migration of the planet-Trojan system, and formation in the inner part of the protoplanetary disk followed by capture in a 1:1 MMR during the migration of a giant planet. As these scenarios are general, they present variety of possibilities for incorporating formation, migration, and capture mechanisms into a single model. We refer the reader to studies by Laughlin and Chambers (2002), Chiang and Lithwick (2005), Thommes (2005), Cresswell and Nelson (2006), Beaugé et al (2007), Morbidelli et al (2008), Hadjidemetriou and Voyatzis (2011), and Giuppone et al (2012) for more details on the models of Trojan planet formation, and the current state of research on this topic.

Acknowledgements NH acknowledges support from NASA EXOB grant NNX09AN05G, the NASA Astrobiology Institute under Cooperative Agreement NNA09DA77A at the Institute for Astronomy (IfA), University of Hawaii, and Alexander von Humboldt Foundation. NH is also thankful to the Computational Physics group at the Institute for Astronomy and Astrophysics, University of Tübingen for their kind hospitality during the course of this project. SC acknowledges support from the IfA NSF-funded REU program. TCH acknowledges support from the Korea Astronomy and Space Science Institute (KASI) grant 2012-1-410-02 and the Korea Research Council for Fundamental Science and Technology (KRCF) through the Young Research Scientist Fellowship Program. The MEGNO computations were carried out at the SFI/HEA Irish Center for High-End Computing (ICHEC) Center and the PLUTO computing cluster at KASI. TCH would also like to thank the Institute for Astronomy and the NASA Astrobiology Institute at the University of Hawaii-Manoa for their hospitality during the course of this project.

References

1. Agol, E., Steffen, J., Saari, R. and Clarkson, W.: On detecting terrestrial planets with timing of giant planet transits, *MNRAS*, **359**, 567-579 (2005)
2. Agol, E. and Steffen, J. H.: A limit on the presence of Earth-mass planets around a Sun-like star, *MNRAS*, **374**, 941-948 (2007)
3. Beaugé, C., Sándor, Zs., Érdi, B. and Süli, Á.: Co-Orbital Terrestrial Planets in Exoplanetary Systems: a Formation Scenario, *A & A*, **463**, 359-367 (2007)
4. Chambers, J. E.: A hybrid symplectic integrator that permits close encounters between massive bodies, *MNRAS*, **304**, 793-799 (1999)
5. Chiang, E. I. and Lithwick, Y.: Neptune Trojans as a Test Bed for Planet Formation, *ApJ*, **628**, 520-532 (2005)
6. Cincotta, P. M. and Simó, C.: Simple Tools to Study Global Dynamics in Non-Axisymmetric Galactic Potentials - I, *A & A Suppl.*, **147**, 205-228 (2000)
7. Cresswell, P. and Nelson, R. P.: On the Evolution of Multiple Protoplanets Embedded in a Protostellar Disc, *A & A*, **450**, 833-853 (2006)

8. Deeg, H. J.: Detection of Terrestrial Planets and Moons with the Photometric Transit Method, In: B. Foing and B. Battrick (eds) Earth-like planets and moons. Proceedings of the 36th ESLAB Symposium, pp. 237-243, ESA Publications Division, Noordwijk (2002)
9. Ford, E. B. and Gaudi, B. S.: Observational Constraints on Trojans of Transiting Extrasolar Planets, *ApJ*, **652**, L137-L140 (2006)
10. Ford, E. B. and Holman, M. J.: Using Transit Timing Observations to Search for Trojans of Transiting Extrasolar Planets, **664**, L51-L54 (2007)
11. Ford, N. et al.: Transit Timing Observations From *Kepler*. I. Statistical Analysis of the First Four Months, *ApJS*, **197**, article id. 2 (2011)
12. Goździewski, K., Bois, E., Maciejewski, A. J. and Kiseleva-Eggleton, L.: Global Dynamics of Planetary Systems with the MEGNO Criterion, *A & A*, **378**, 569-586 (2001)
13. Giuppone, C. A., Beaugé, C., Michtchenko, T. A. and Ferraz-Mello, S.: Dynamics of two planets in co-orbital motion, *MNRAS*, **407**, 390-398 (2010)
14. Giuppone, C. A., Benítez-Llambay, P. and Beaugé, C.: Origin and Detectability of Co-Orbital Planets from Radial Velocity Data, *MNRAS*, **421**, 356-368 (2012)
15. Hadjidemetriou, J. D., Psychoyos, D. and Voyatzis, G.: The 1/1 resonance in extrasolar planetary systems *CeMDA*, **104**, 23-38 (2009)
16. Hadjidemetriou, J. D. and Voyatzis, G.: The 1/1 Resonance in Extrasolar Systems. Migration from Planetary to Satellite Orbits, *CeMDA*, **111**, 179-199 (2011)
17. Haghighipour, N. and Kirste, S.: On the Detection of (Habitable) Super-Earths Around Low-Mass Stars Using *Kepler* and Transit Timing Variation Method, *Celest. Mech. Dyn. Astr.*, **111**, 267-284 (2011)
18. Heyl, J. S. and Gladman, B. J.: Using long-term transit timing to detect terrestrial planets, *MNRAS*, **377**, 1511-1519 (2007)
19. Holman, M. J. and Murray, N. W.: The use of transit timing to detect terrestrial-mass extrasolar planets, *Science*, **307**, 1288-1291 (2005)
20. Holman, M. J., et al: Kepler-9: A system of multiple planets transiting a sun-like star confirmed by timing variations, *Science*, **330**, 51-54 (2010)
21. Johnson, J. A., et al. : Characterizing the Cool KOIs. II. The M Dwarf KOI-254 and Its Hot Jupiter, *AJ*, **143**, article id. 111 (2012)
22. Kipping, D. M.: Transit timing effects due to an exomoon, *MNRAS*, **396**, 1797-1804 (2009a)
23. Kipping, D. M.: Transit timing effects due to an exomoon - II, *MNRAS*, **392**, 181-189 (2009b)
24. Kipping, D. and Bakos, G.: An independent analysis of Kepler-4b through Kepler-8b, *ApJ*, **730**, id.50 (2011)
25. Laughlin, G. and Chambers, J. E.: Extrasolar Trojans: The Viability and Detectability of Planets in the 1:1 Resonance, *AJ*, **124**, 592-600 (2002)
26. Morbidelli, A., Crida, A., Masset, F. and Nelson, R. P.: Building Giant-Planet Cores at a Planet Trap, *A & A*, **478**, 929-937 (2008)
27. Nesvorný, D. and Morbidelli, A.: Mass and Orbit Determination from Transit Timing Variations of Exoplanets, *ApJ*, **688**, 636-646 (2008)
28. Nesvorný, D.: Transit Timing Variations for Eccentric and Inclined Exoplanets, *ApJ*, **701**, 1116-1122 (2009)
29. Nesvorný, D. and Beaugé, C.: Fast Inversion Method for Determination of Planetary Parameters from Transit Timing Variations, **709**, L44-L48 (2010)

-
30. Nesvorný, D., Kipping, D. M., Buchhave, L. A., Bakos, G. A., Hartman, J. and Schmitt, A. R.: The Detection and Characterization of a nontransiting Planet by Transit Timing Variations, *Science*, **336**, 1133-1136 (2012)
 31. Sartoretti, P. and Schneider, J.: On the Detection of Satellites of Extrasolar Planets with the Method of Transits, *A& A*, **134**, 553-560 (1999)
 32. Simon, A., Szatmáry, K. and Szabó, Gy. M.: Determination of the size, mass, and density of “exomoons” from photometric transit timing variations, *A& A*, **470**, 727-731 (2007)
 33. Steffen, J. H. and Agol, E.: An analysis of the transit times of TrES-1b, *MNRAS*, **364**, L96-L100 (2005)
 34. Thommes, E. W.: A Safety Net for Fast Migrators: Interactions Between Gap-Opening and Sub-Gap-Opening Bodies in a Protoplanetary Disk, *ApJ*, **626**, 1033-1044 (2005)
 35. Veras, D., Ford, E. B. and Payne, M. J.: Quantifying the challenges of detecting unseen planetary companions with transit timing variations, *ApJ*, **727**, article id.74 (2011)

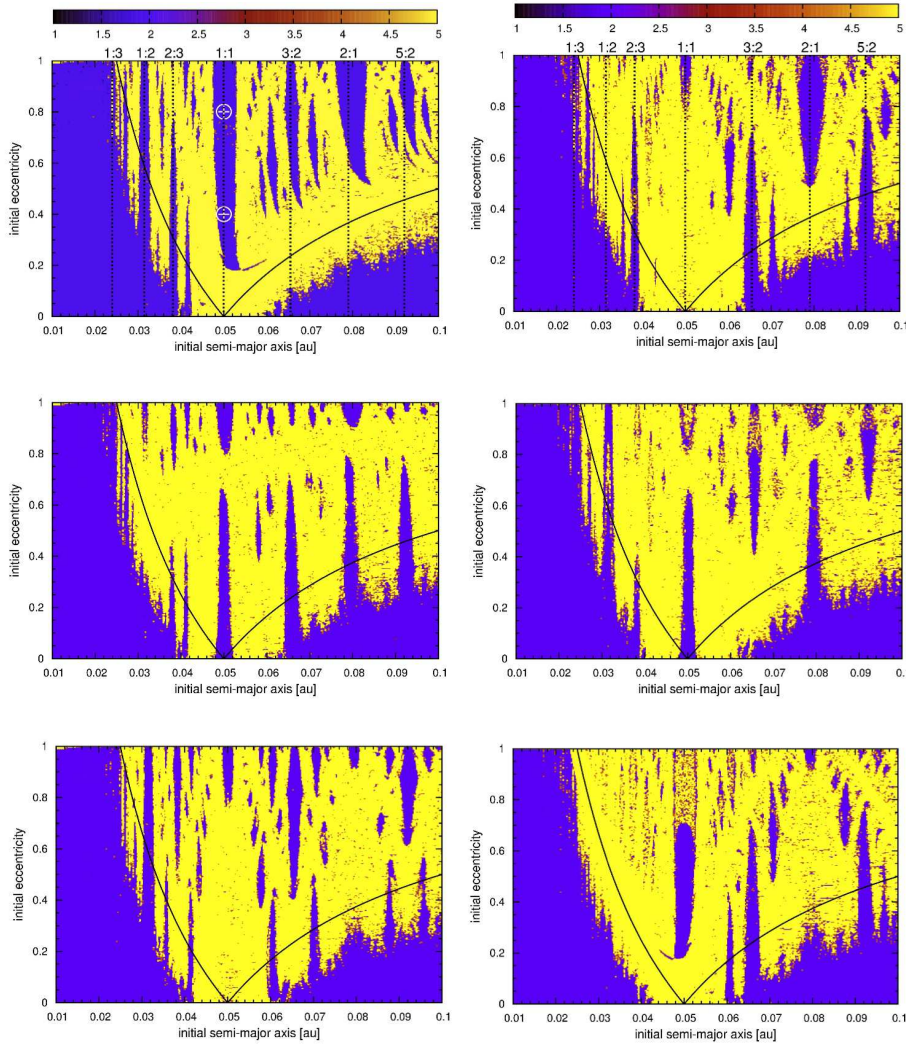


Fig. 1 MEGNO dynamical maps for an Earth-mass perturbing planet in a system consisting of a solar-mass star and a Jupiter-mass transiting body. The vertical and horizontal axes show the initial values of the orbital eccentricity and semimajor axis of the Earth-mass planet. The transiting planet is in a 4-day orbit and was initially started with no eccentricity. The black curves show the loci of points whose perihelion/aphelion distances are 0.05 AU from the central star. The color-coding shows the value of MEGNO from 1 corresponding to a regular orbit to 5 indicating chaotic behavior. Each panel corresponds to a different combination of the initial mean-anomaly of the transiting and perturbing planets. In the panels on the left (right), the initial mean-anomaly of the Earth-mass perturber was set to zero (180°) and the mean-anomaly of the transiting planet was 0 (top), 90° (middle), and 180° (bottom), respectively. Several islands of stability corresponding to mean-motion resonances between the two planets are also shown.

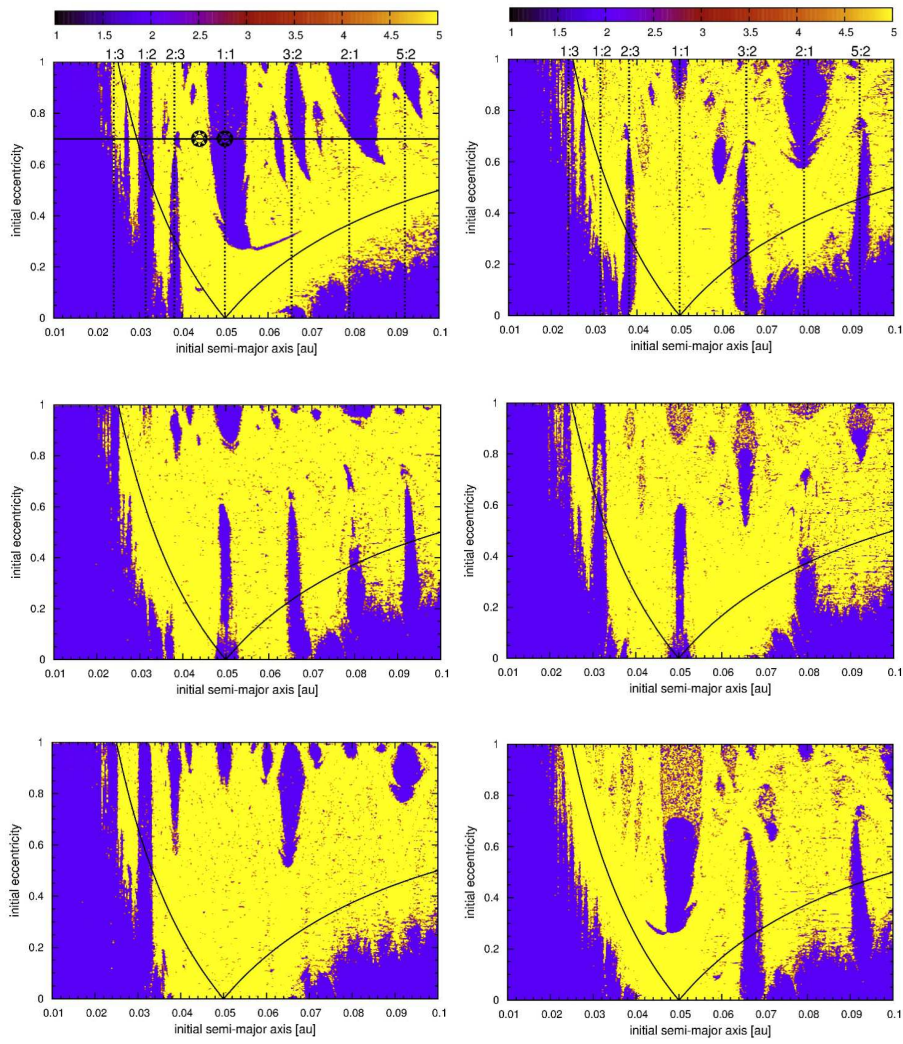


Fig. 2 MEGNO dynamical maps similar to Figure 1 for a 0.3 solar-mass star. The giant planet is in a 7.5-day orbit.

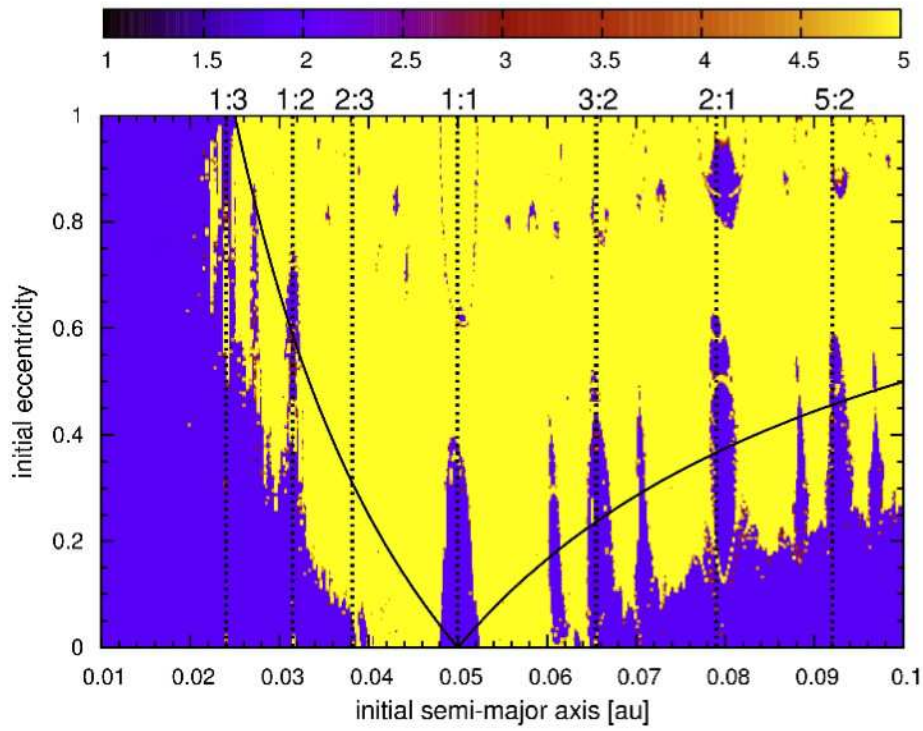


Fig. 3 MEGNO dynamical map similar to top-left panel of figure 1 for an Earth-mass planet with an initial argument of pericenter of 60° . As shown here, the Trojan planet has a stable orbit for the initial values of its orbital eccentricity small than ~ 0.35 .

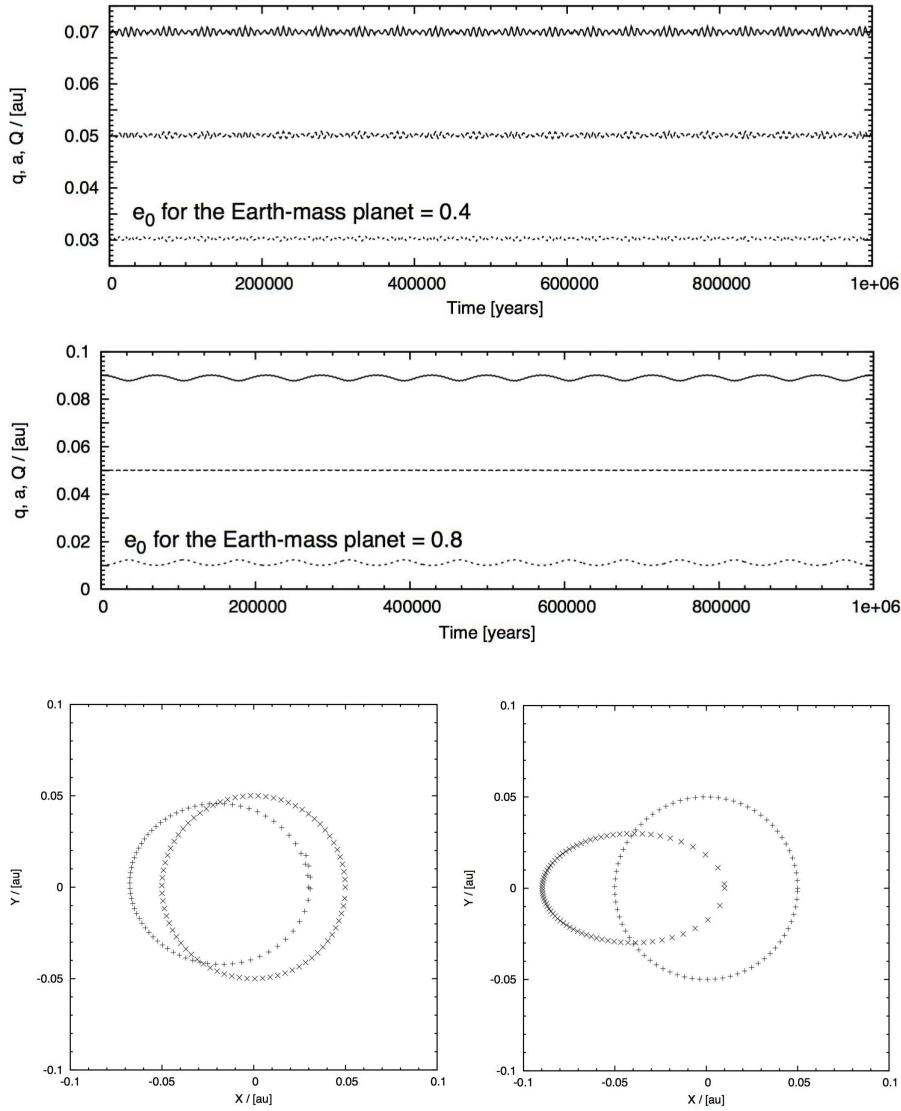


Fig. 4 Top: Graph of the semimajor axis (a), perihelion (q), and aphelion (Q) distances of an Earth-mass perturber in the system of figure 1. The initial eccentricity of the Earth-mass planet was 0.4 corresponding to the lower white cross in the 1:1 MMR region of the top-left panel of figure 1. Middle: Similar graph as in the top panel where the initial eccentricity of the Earth-mass planet was 0.8. The orbit of this planet corresponds to the upper white cross in the 1:1 MMR region of the top-left panel of figure 1. Bottom: The astrocetric orbits of the transiting giant planet and the Trojan perturber showing only one orbit. The bottom-left panel corresponds to the system of the top graph, and the bottom-right panel is for the system of the middle graph.

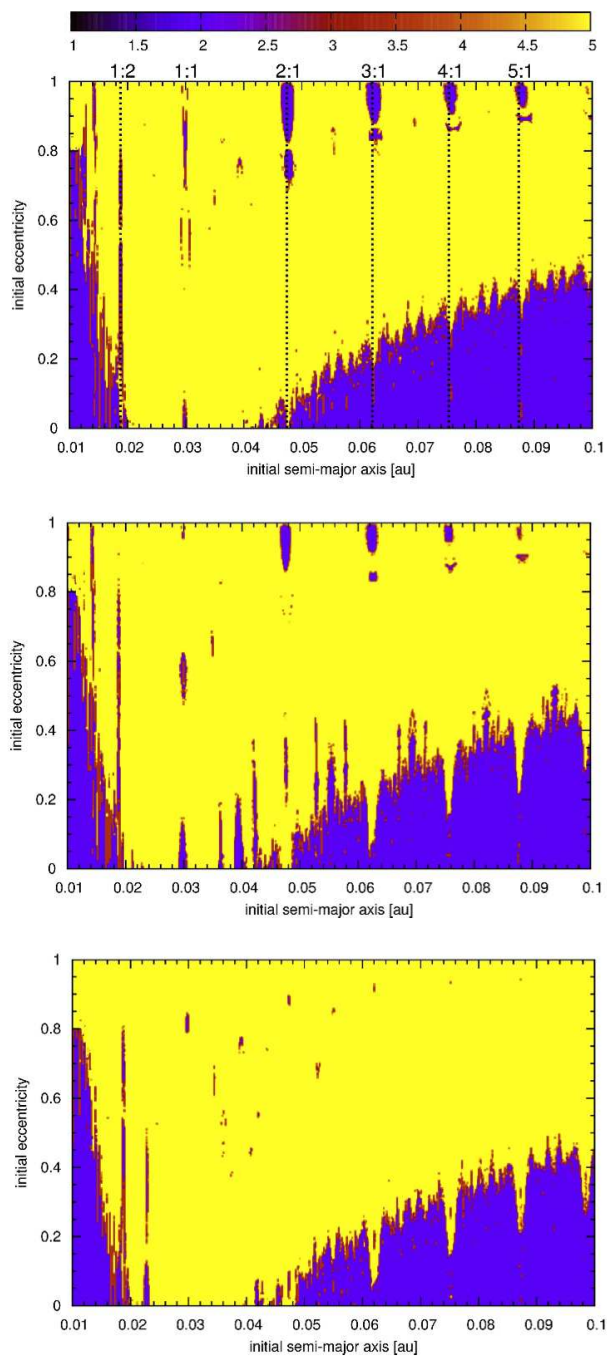


Fig. 5 MEGNO dynamical maps for an Earth-mass perturber in the transiting system of KOI-254. The initial orbital elements of the transiting planet, KOI-254 b (0.505 Jupiter-mass), have been taken from Johnson et al (2012). The Earth-mass perturber was initially in a circular orbit with a radius equal to that of the transiting planet. Its angular orbital elements were initially set to zero. The initial mean anomaly of the transiting planet was set to 90° (top), 180° (middle), and 270° (bottom). In the top panel, the 2:1, 3:1, 4:1, and 5:1 MMRs have widths of 0.0020, 0.0022, 0.00215, and 0.00158 AU, respectively.

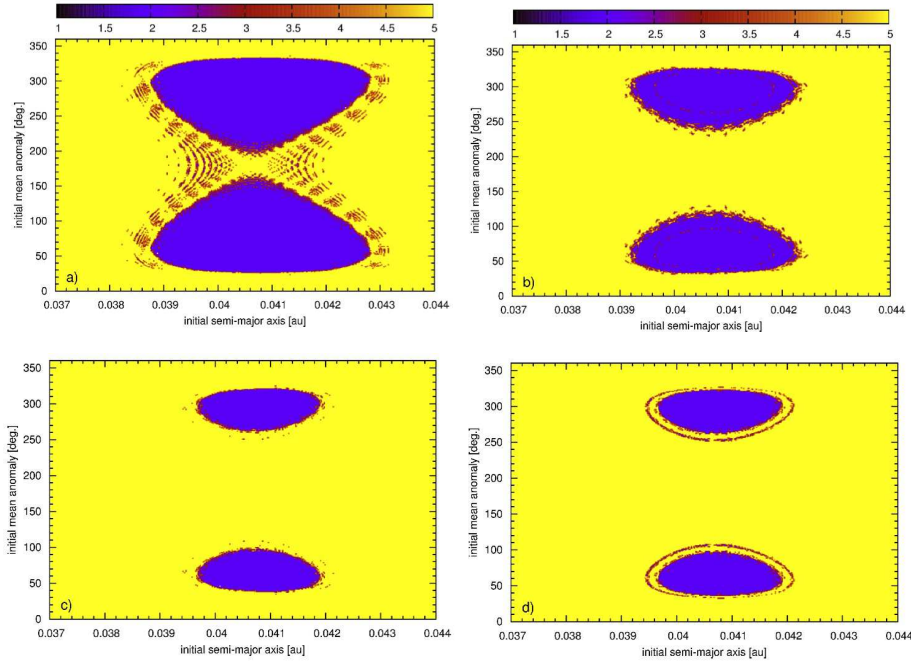


Fig. 6 MEGNO dynamical maps for an Earth-mass Trojan in a system consisting of a Jupiter-mass transiting planet in a 3-day orbit and a solar-mass star. The initial eccentricities of the (transiting , Trojan) planets were set to $(0, 0)$ for the top-left panel, $(0, 0.1)$ for the top-right panel, $(0.1, 0)$ for the bottom-left panel, and $(0.1, 0.1)$ for the bottom-right panel, respectively.

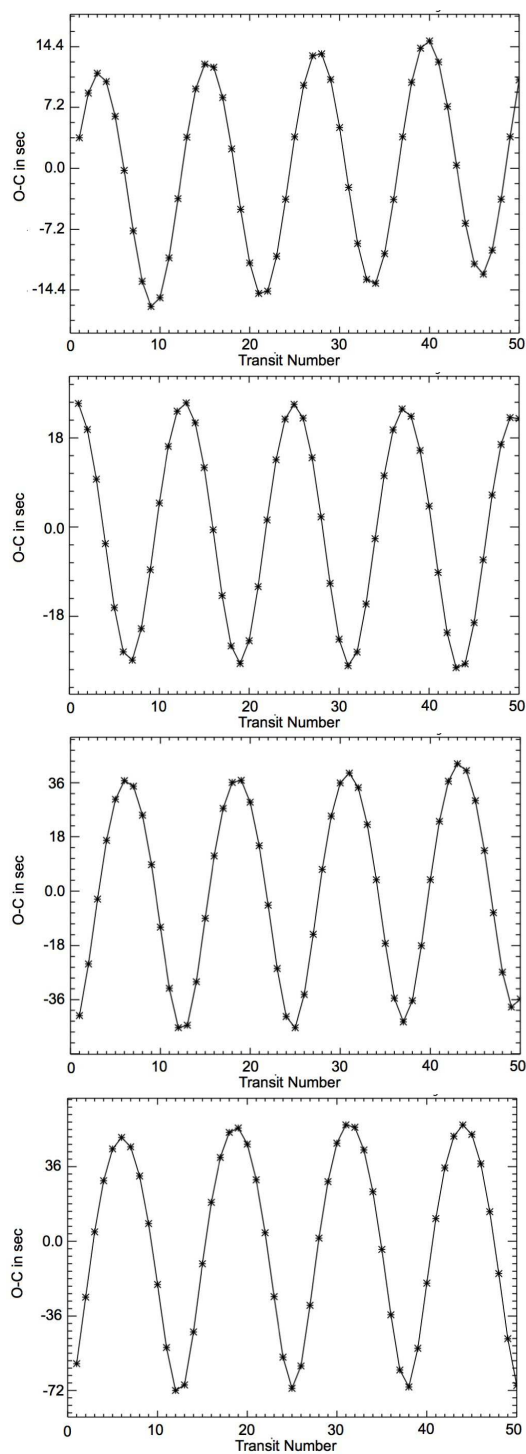


Fig. 7 Graphs of the TTVs of a Jupiter-mass transiting planet due to an Earth-mass Trojan. The central star is Sun-like and the transiting planet is in a 3-day, circular orbit. The initial orbital eccentricity of the Trojan planet was 0 (top-left), 0.05 (top-right), 0.1 (bottom-left), and 0.15 (bottom-right). As shown here, the amplitude of TTVs increase by increasing the eccentricity of the Trojan planet from ~ 16 s for zero eccentricity to ~ 72 s for an eccentricity of 0.1.

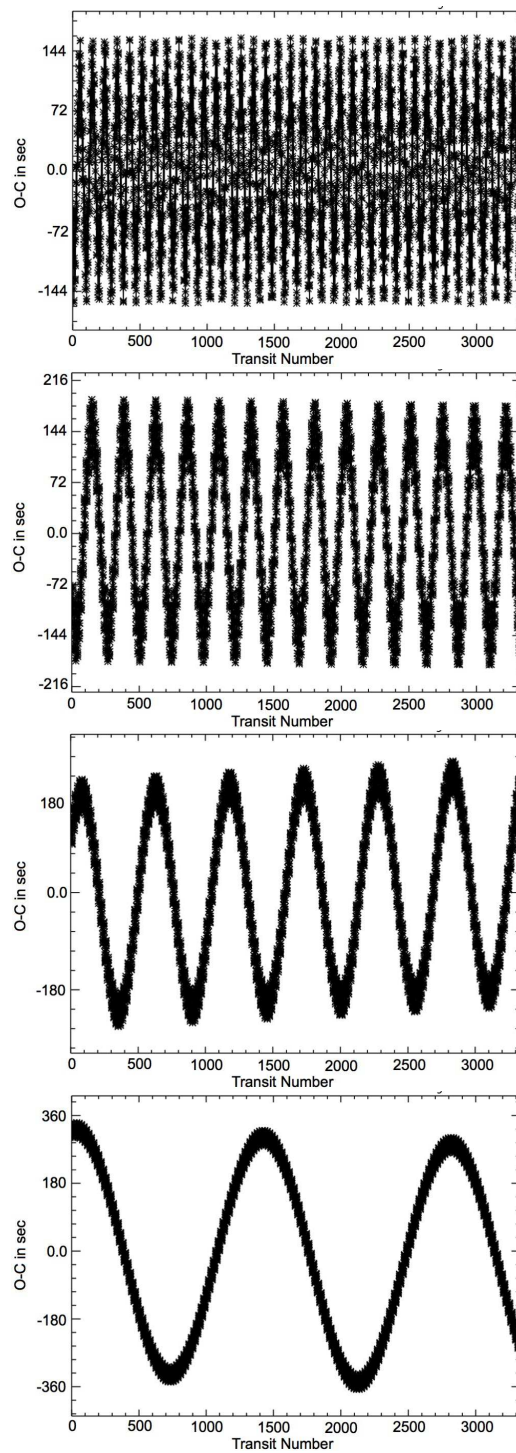


Fig. 8 Graphs of the TTVs of a Jupiter-mass transiting planet in a 3-day, circular orbit due to an Earth-mass perturber in a 1:1 MMR. The central star is solar-mass. The perturber's orbital eccentricity is equal to 0.4 (top-left), 0.5 (top-right), 0.6 (bottom-left), and 0.7 (bottom-right). Note that the time of integration is over three years. As shown by the bottom-right panel, the amplitude of TTV increases to approximately 6 minutes; a value that is within the range of the detected transit timing variations of the *Kepler*'s planetary candidates.

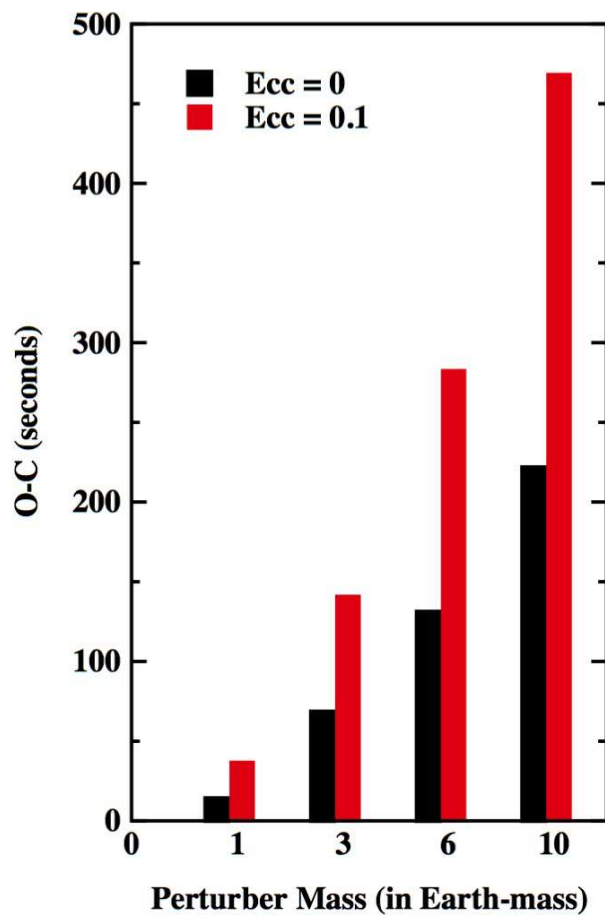


Fig. 9 Graph of the maximum TTVs for different value of the mass of the Trojan perturber. The central star is solar-type and the transiting planet is Jupiter mass in a 3-day, circular orbit. The black and red colors correspond to different initial orbital eccentricity of the Trojan planet. As expected, the amplitude of TTVs increase for larger values of the mass of this object.

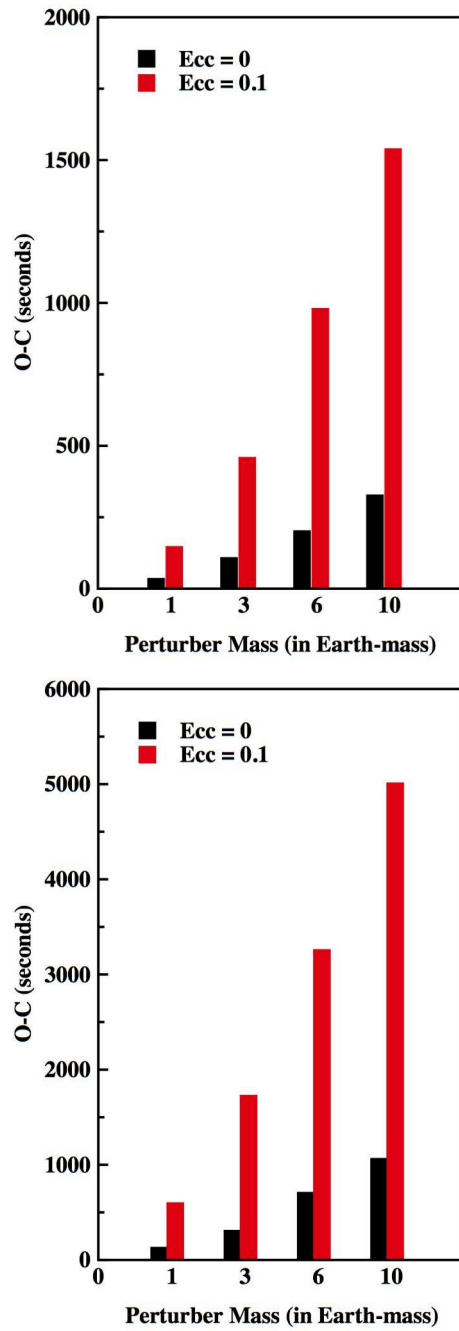


Fig. 10 Graphs of the TTVs of a 0.1 Jupiter-mass (left) and 0.5 Jupiter-mass (right) transiting planet due to a Trojan with a mass from 1 to 10 Earth-masses. The black and red colors correspond to different initial orbital eccentricity of the Trojan planet. The transiting planet was initially in a circular orbit and the central star is Sun-like.

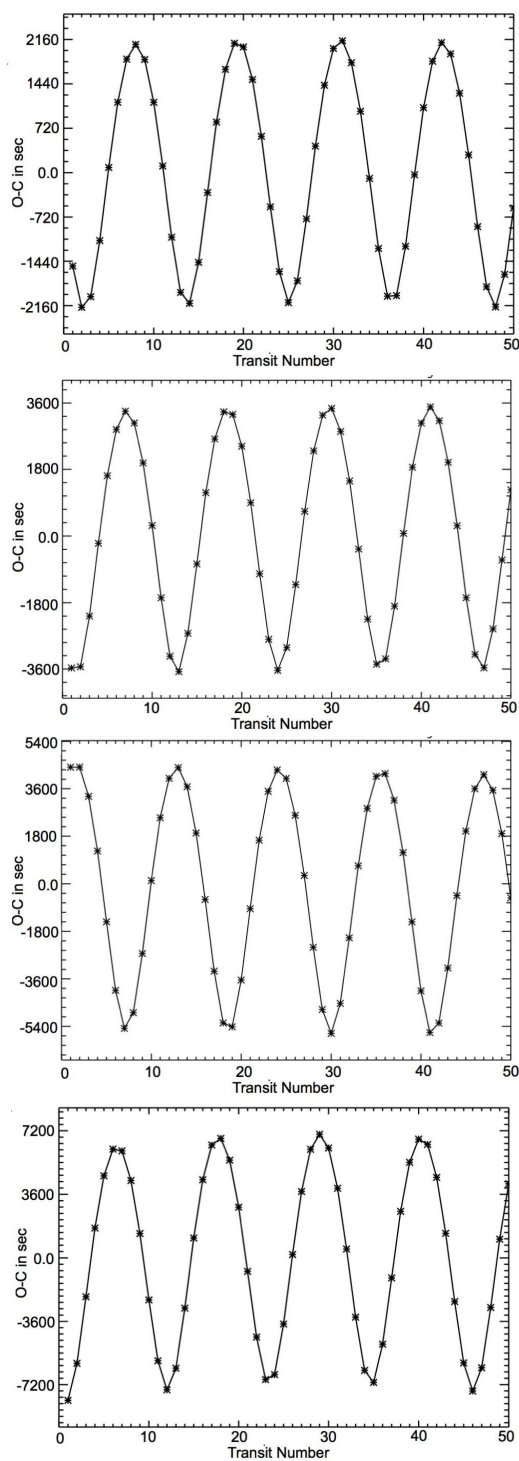


Fig. 11 Graphs of the amplitudes of the TTVs of a 0.1 Jupiter-mass transiting planet due to a 6 Earth-masses Trojan perturber. The transiting planet is in a circular orbit and the central star is Sun-like. From top to bottom and clock-wise, the graphs correspond to the transiting planet in a 3-day (top-left), 5-day (top-right), 7-day (bottom-left), and 10-day (bottom-right) orbits.

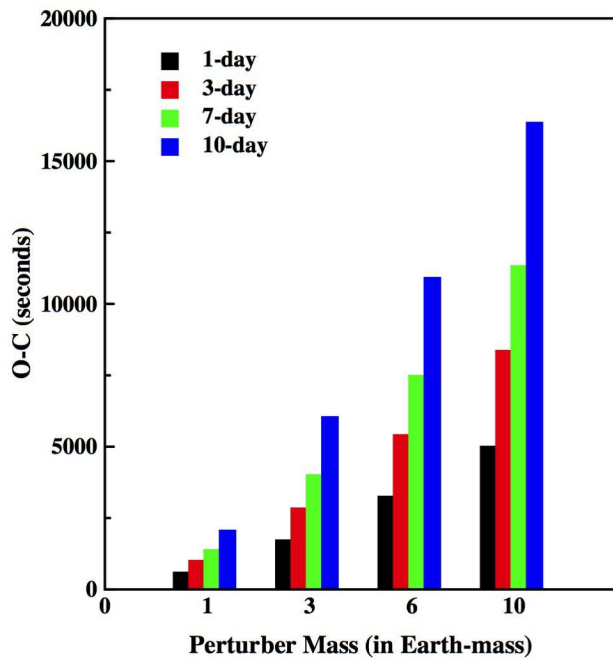


Fig. 12 Graph of the maximum value of the TTV of a 0.1 Jupiter-mass transiting planet due to a Trojan perturber with a mass from 1 to 10 Earth-masses. The transiting planet is in a circular orbit and the central star is Sun-like. The colors corresponds to different orbital period of the transiting planet.

5 Appendix

In general, determining the actual dynamical state of an object using MEGNO maps requires long-term integrations. This is due to the fact that the detection of chaos with MEGNO depends strongly on the length of the overall integration time, and as a result, integrating for long times become crucial for obtaining the true dynamical picture of the underlying structure of the phase space. Long-term integrations are particularly important when attempting to detect chaotic (secular and mean-motion) orbital resonances. To determine to what extent the MEGNO maps of our systems represent the true dynamical stability of the perturber, we considered a very narrow range of orbital eccentricity, $e = 0.7$, (the black horizontal line in the top-left panel of figure 2 in the main text) and calculated a one-dimensional MEGNO over the range of the perturber’s semimajor axis, and for longer times. Figure 1 shows the results of three different integration time spans, 100 years (top), 1000 years (middle), and 10,000 years (bottom). We considered three different integrations times in order to be able to study the evolution of the MEGNO and determine the time beyond which the structure of the phase space will stay unchanged. For instance, an inspection of the panels in this figure shows that the initial conditions at the point 0.0435 AU at the top and middle panels are quasi-periodic approaching a MEGNO of 2. However, as the integrations continue, the quasi-periodic nature of this point disappears and it becomes unstable. Our integrations indicated that 10,000 years would be sufficiently long to capture a close-to-complete qualitative picture of the dynamical state of the perturber. After this time, the maps maintained their architecture and did not change, suggesting that their depicted orbital (ir)regularity is a true representation of the dynamical (in)stability of the system. Figures 2 and 3 show samples of the results as examples of the quasi-periodic (stable) and chaotic (in this case, unstable) orbits.

The initial values of the eccentricity and semimajor axis of the perturber for these figures are shown by black crosses in the top-left panel of figure 2 in the main text. Figure 2 shows details of the time evolution of MEGNO for a quasi-periodic (stable) initial condition (the black cross from the low-MEGNO region around the 1:1 MMR). As shown here, the value of MEGNO approaches 2.0 asymptotically and stays in that level for the remainder of the integrations. The perturber corresponding to figure 3, however, shows an entirely different behavior. The integrations of the orbit of this object, whose initial semimajor axis was chosen from the high-MEGNO part of the upper left panel of figure 2 in the main text, indicate that the eccentricity of its orbit rapidly increases causing the object to collide with the central body in a short time. As expected, the magnitude of the MEGNO of this body also reaches very high values during this time.

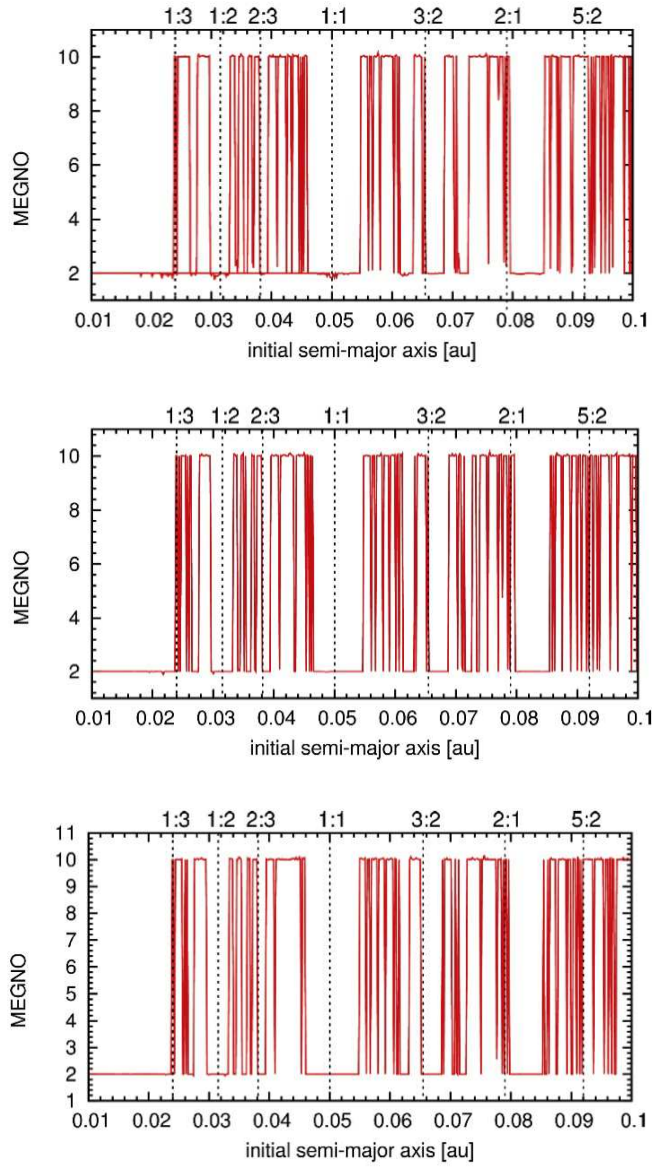


Fig. 13 One-dimensional MEGNO maps for an Earth-mass perturber in the system of figure 2 in the main text. The initial eccentricity of the perturber was 0.7. See the black horizontal line on the top-left panel of figure 2. The panels show the MEGNO for different times of integration; 100 years (top), 1000 years (middle), and 10,000 years (bottom). As shown here, when the integration reaches long times, the MEGNO maps do not change indicating that their regions of regular orbits represent actual stability of the perturbing planet.

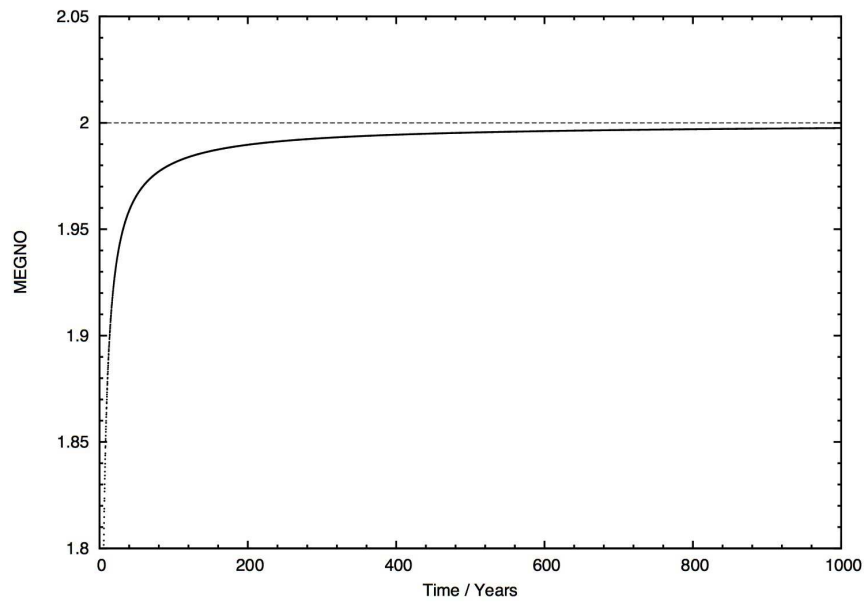


Fig. 14 The graph of the value of the MEGNO of an Earth-mass perturber shown by the black cross in the low-MEGNO region of the 1:1 MMR in the upper left panel of figure 2 in the main text. As shown here, at the beginning of the integration, the value of the MEGNO of the planet rapidly approaches 2 and stays in that level for the rest of the integration indicating that the orbit of the planet is long-term stable.

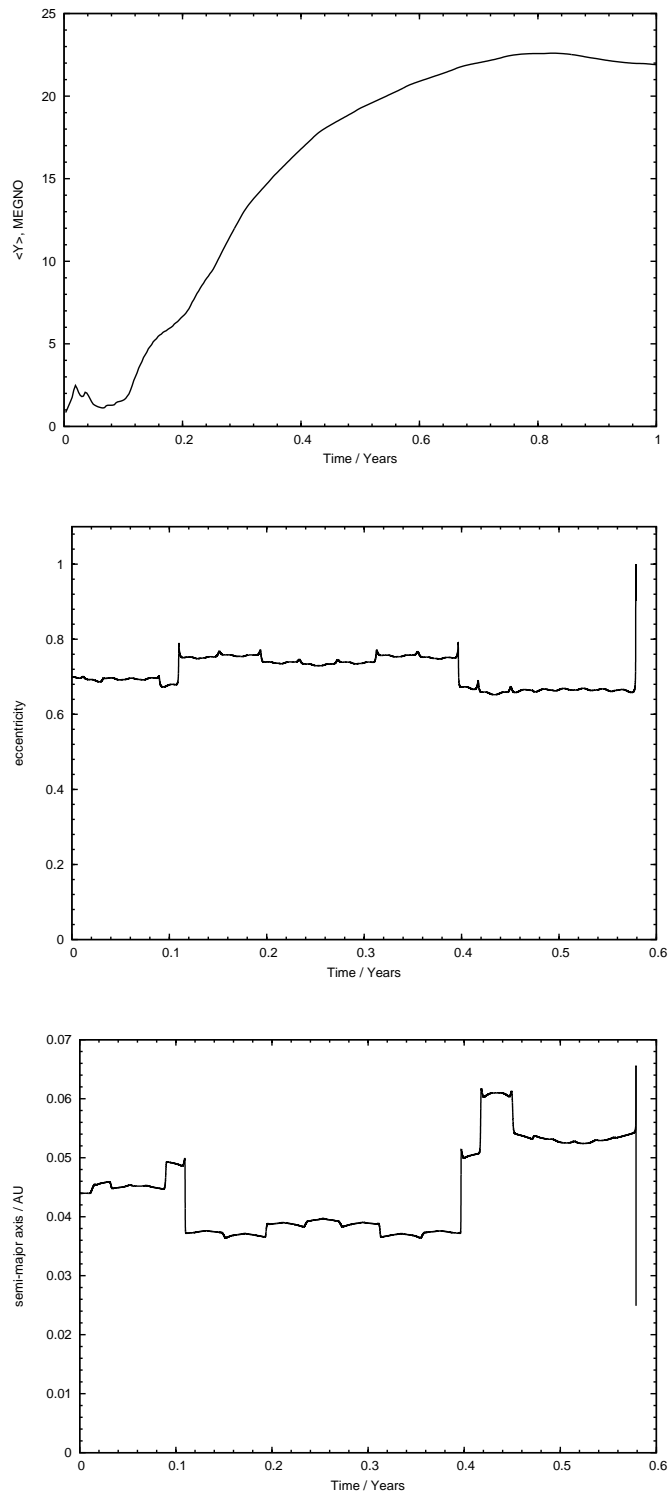


Fig. 15 Graphs of the MEGNO, eccentricity and semimajor axis of the Earth-mass perturber indicated by the left black cross in the top-left panel of figure 2 in the main text. As shown here, the planet's orbit becomes unstable shortly after the start of the integrations when it collides with the central star. As expected, the magnitude of the MEGNO of the planet raises to very high values during this time.